Chemical Science

EDGE ARTICLE

View Article Online
View Journal | View Issue

Cite this: *Chem. Sci.*, 2014, **5**, 4017

Oxygen chemisorption/desorption in a reversible single-crystal-to-single-crystal transformation†

Jonas Sundberg,[a] Lisa J. Cameron,[b] Peter D. Southon,[b] Cameron J. Kepert[b] and Christine J. McKenzie*[a]

Crystalline salts of a series of cationic multimetallic cobalt complexes reversibly, selectively and stoichiometrically chemisorb dioxygen in a process involving the two electron oxidation of dimetallic sites with concurrent reduction of two equivalents of sorbed O_2 to form μ-η^1,η^2-peroxide ligands. The coordinating ability of counteranions, ClO_4^-, PF_6^-, BF_4^-, $CF_3SO_3^-$ and NO_3^- determine the O_2 affinity of the deoxygenated forms, and the nitrate and triflate salts sorb dioxygen at a significantly slower rate compared to the PF_6^- and BF_4^- salts (hours *versus* sub-seconds at ambient temperature and pressure). Single crystal X-ray structural determination for a nitrate salt of the 2-aminoterephthalato-linked deoxy system, $[\{(bpbp)Co_2^{II}(NO_3)\}_2(NH_2bdc)](NO_3)_2\cdot 2H_2O$ ($bpbp^-$ = 2,6-bis(*N*,*N*-bis(2-pyridylmethyl)-aminomethyl)-4-*tert*-butylphenolato, NH_2bdc^{2-} = 2-amino-1,4-benzenedicarboxylato) shows that nitrate ions are coordinated as bridging ligands. These crystals undergo reversible single-crystal-to-single-crystal (SC-to-SC) transformations on the stoichiometric uptake of O_2. During this process O_2 replaces the two nitrate ligands. Thus the Co ions are six coordinated in both the oxy and deoxy states. This SC-to-SC process involves the concerted fast migration of neutral dioxygen through the crystal lattice and the translational movement by 4–6 Å of at least two of nitrate anions. Rapid hydration/dehydration processes involving several molecules of co-crystallized water per unit cell accompany the reaction. Besides large atom movements involving O_2, NO_3^- and H_2O, these impressive examples of consecutive SC-to-SC-to-SC transformations involve *the cleavage of four bonds*, and the *creation of four new bonds*, in one single molecule. The solid state structural rearrangements observed provide an explanation for the slower rates of dioxygen uptake for the complexes isolated as nitrate salts, and by inference, the triflate salts, compared to the salts of more weakly coordinating counteranions, ClO_4^-, PF_6^- and BF_4^-.

Received 3rd June 2014
Accepted 11th July 2014

DOI: 10.1039/c4sc01636j

www.rsc.org/chemicalscience

Introduction

Reactions of dioxygen are essential in a wide range of biological and chemical processes: the reversible binding of dioxygen, its activation in order to prime it for the oxidation of substrates, and its release after formation. The presence of paramagnetic states of iron, copper, nickel and manganese in enzymes like hemoglobin, hemerythrin, hemocyanin, cytochrome P450s, superoxide dismustases and the Oxygen Evolving Center in photosynthesis is essential. The risk of formation of reactive oxygen species, and possible consequent non-specific chain reactions, mean that the metal-based redox reactions must be very finely adjusted to prevent one electron transfers and possible release of cytotoxic superoxide. O_2 binding by metalloenzymes can be regarded as a highly selective "chemisorptive process", *i.e.*, bond formation occurs between the O_2 and the metal co-factors. The separation of O_2 from other gases by reversible sorption is similarly essential for many industrial processes. However, efficiency and selectivity equal to biological processes has not yet been achieved. While O_2 concentration by sorptive materials is potentially less energy intensive compared with cryogenic distillation, currently this method can be used only in applications where it is not required in higher purity. These processes, based on zeolite materials,[1] are physisorptive in contrast to the aforementioned biological reactions.[2] Solid state metal–organic compounds offer a chemical middle ground between dynamic and flexible enzymes and rigid inorganic zeolites for the design of materials capable of performing reversible O_2 binding. An obvious place to start in the design of these materials is by exploiting coordination complexes which are known to perform this task in the solution state. Co and Ir complexes, *e.g.* Co(salen)[3] and Vaska's[4] complex, have been long

[a]*Department of Physics, Chemistry and Pharmacy, University of Southern Denmark, Campusvej 55, 5230 Odense M, Denmark. E-mail: mckenzie@sdu.dk; Fax: +45 6615 8760; Tel: +45 6550 2518*

[b]*School of Chemistry, The University of Sydney, NSW 2006, Australia*

† Electronic supplementary information (ESI) available: Supporting figures, Table of selected bond distances and angles. IR spectra. CCDC 1006439 and 1006440. For ESI and crystallographic data in CIF or other electronic format see DOI: 10.1039/c4sc01636j

recognised as capable of oxidative addition and reductive elimination of O_2 in solution as they cycle between M(I) and M(III) oxidation states.[5] Thus it is not surprising that the immobilisation of these types of complexes in membranes[6] and polymers,[7] with the intention that practical materials and devices for O_2 separation processes might be constructed, has been pursued. However, none of these systems has achieved the O_2 binding active site concentration, nor the reversibility of $[\{(bpbp)Co_2^{III}(O_2)\}_2(bdc)](PF_6)_4$ ($bpbp^-$ = 2,6-bis(*N*,*N*-bis(2-pyridylmethyl)aminomethyl)-4-*tert*-butylphenolato, bdc^{2-} = 1,4-benzenedicarboxylato). The cation in this compound is shown in Scheme 1, structure **2a**. The deoxy form, $\mathbf{2a_{deoxy}}(PF_6)_4$ reversibly binds O_2 from air in the solid state with affinities equalling that of myoglobin.[8] The O_2 sorption/desorption process of this compound can be cycled many times without any loss of activity. Solid $\mathbf{2a}(PF_6)_4\cdot 3H_2O$ concentrates O_2 by a factor of 32 times the density of O_2 gas at 1 atm, or 160 times that in air. Apart from a higher capacity than the zeolites currently used on industrial scale for a far less efficient O_2 concentration, what is very interesting is the extreme affinity that this material shows for O_2. At room temperature an excess of the material will reversibly remove more than 99% of oxygen from the air with a 38 fold selectivity factor for O_2 over N_2. Compared to recently discovered systems showing selectivity for O_2 uptake, this is almost double that of the dichromium(II)tetracarboxylate paddlewheel based metal–organic framework,[9] and almost four times higher than the coordination network Fe_2(dobdc) (dobdc^{4-} = 2,5-dioxido-1,4-benzenedicarboxylate) (MOF-74).[10] Despite not being polymeric, $\mathbf{2a}(PF_6)_4\cdot 3H_2O$ also shows greater stability towards irreversible redox processes. While the oxy $\mathbf{2a}(PF_6)_4\cdot 3H_2O$ has been structurally characterized, the deoxy and by its nature, air sensitive form, $\mathbf{2a_{deoxy}}(PF_6)_4$, has not.

In solution, the O_2 affinity of a series of parent dinuclear complexes, Scheme 1, structures **1a–e**, is tuned by the substitutions on the basic framework using electron donating or withdrawing groups on the carboxylate co-ligand.[11] Thus for every chloro group introduced onto the acetato bridge the O_2 affinity is reduced. The O_2 affinities for **1a–e** ranged from similar to myoglobin through to haemoglobin respectively. Conversely, when a dicobalt complex was anchored to gold surfaces using **1f**, the O_2 affinity was increased so much that the system is no longer an effective reversible O_2 binder.[12] With a view to practical applications the motivation for the work described in this report was carried out to ascertain whether or not this considerable range of solution state tunability could be translated into the solid state. With readily tuneable solid state materials on hand it is possible to imagine the construction of systems, capable not only of O_2 storage, but through layering, also of the vectorial transport of this biologically and industrially important molecule.

Results and discussion

Synthesis

The cationic oxy complexes depicted in Scheme 1 (**1a–e** and **2a**) were previously isolated for the most part as perchlorate salts. The safety issues associated with the need for heating solid samples for the present study forced the preparation of alternative formulations. We have now synthesized **2a** as two new salts along with relatives which are functionalized on the bdc^{2-} linker (**2b–d**) as hexafluorophosphate, tetrafluoroborate, triflate and nitrate salts. Typically the dinucleating pro-ligand, bpbpH, the appropriate carboxylic acid and base were mixed in stoichiometric amounts in mixtures of methanol, acetone and H_2O under aerobic conditions. This reaction results in dark solutions from which the near black Co(III) oxy forms (as depicted in Scheme 1) crystallize over hours to days. The production of crystalline materials was crucial for the observation of consistent sorption/desorption properties, suggesting that solid phase structure plays an important role in the chemisorptive properties of these materials. Rapid precipitation formed light brown amorphous powders, which were inactive or only minimally active towards reversible O_2 binding. Apart from an apparent need for crystalline materials, and therewith highly regular 3D structures, a possible explanation for the colour and low O_2 uptake is contamination by "met" ($Co(II)_2$ to $Co(III)_2$-based oxidation only-no O_2 binding and reduction) forms in which the carboxylato ligands are replaced by hydroxido.[13] On heating, the crystalline materials change to a pink colour due to the loss of O_2 and the generation of "deoxy" materials containing the counterpart $Co(II)_4$-containing $\mathbf{1a–e_{deoxy}}$ and $\mathbf{2a–d_{deoxy}}$ (not shown in Scheme 1). On cooling back to room temperature the dark colour re-emerges as the materials chemisorb O_2 from the air to form the $Co(III)_4$ oxy materials **1a–e** and **2a–d**. This process was mostly accompanied by loss of crystal integrity, apart from one case, *vide infra*.

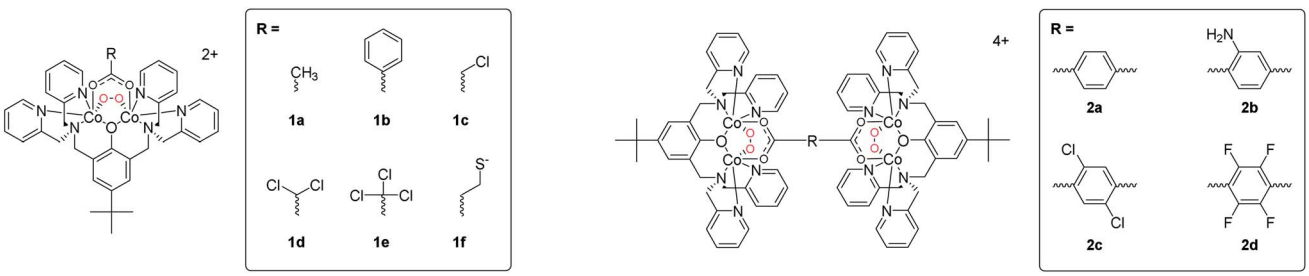

Scheme 1 Chemical structures of the cations in $[(bpbp)Co_2(O_2)(O_2CR)](A)_2$ and $[\{(bpbp)Co_2(O_2)\}_2(bdcR_4)](A)_4$. Counteranions (A): ClO_4^-, PF_6^-, BF_4^-, $CF_3SO_3^-$, NO_3^-.

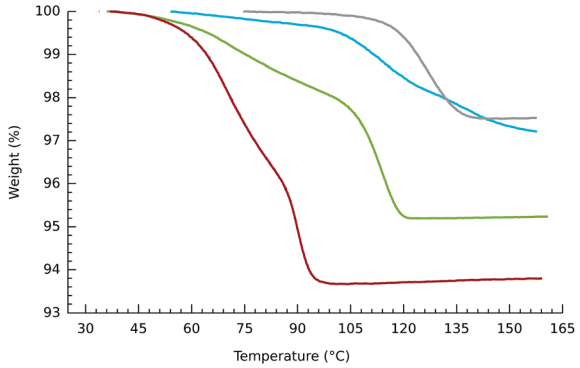

Fig. 1 Thermogravimetric plot for NO_3^- (red), BF_4^- (green), PF_6^- (blue) and $CF_3SO_3^-$ (grey) salts of $[\{(bpbp)Co_2(O_2)\}_2(bdc)]^{4+}$ (**2a**) showing temperature dependent deoxygenation, accompanied by dehydration, see text.

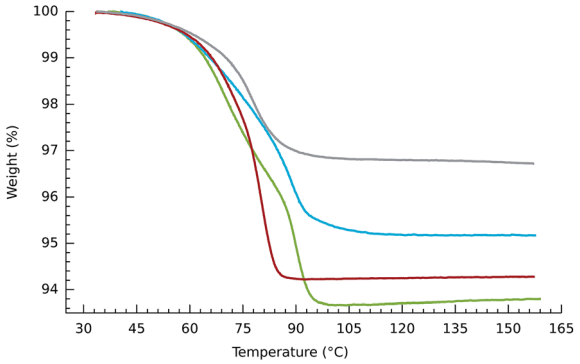

Fig. 3 TGA comparison for $[\{(bpbp)Co_2(O_2)\}_2(bdcR_4)](NO_3)_4 \cdot xH_2O$, $bdcR_4^{2-} = Cl_2bdc^{2-}$ (red, **2c**), bdc^{2-} (green, **2a**), NH_2bdc^{2-} (blue, **2b**) and F_4bdc^{2-} (grey, **2d**) showing temperature difference in deoxygenation and dehydration.

Thermogravimetry

The tetracobalt series **2**, varied systematically with respect to counteranions and substitution on the benzene unit of the bdc^{2-} co-ligand, show slight variation in the temperatures at which the samples of crystalline compounds release O_2. Thermogravimetric plots of O_2 release are shown in Fig. 1–3. Oxygen desorption for the parent $[\{(bpbp)Co_2^{III}(O_2)\}_2(bdc)]^{4+}$, crystallized with four different counteranions, was measured by heating up to 160 °C at 5° min^{-1} under a steady flow of N_2 gas. Elemental analyses indicate that the materials can contain significant and variable amounts of co-crystallized water and other solvent molecules as confirmed in the structurally characterised ClO_4^-,[14] PF_6^-,[8] and NO_3^- salts, *vide infra*. This complicates the interpretation of measurements, however, O_2 desorption appears to be complete for all samples. As seen in Fig. 1 the samples of the triflate and the hexafluorophosphate salts used for the experiments do not appear to contain any co-crystallized solvent. A more obvious two-stage process of guest removal is evidenced by inflections in the TGA curves for the BF_4^- and NO_3^- salts, which may correspond to successive removal of water and oxygen with weight losses corresponding to two and four water molecules respectively. At approximately 100 °C the nitrate salt has lost both O_2 molecules, whereas the PF_6^- salt is completely deoxygenated first at 160 °C. Perhaps consistently, dioxygen resorption is significantly faster for the PF_6^- and BF_4^- salts where it is immediate upon exposure to air. Fig. 2 shows multiple cycles of O_2 desorption and resorption into $\mathbf{2a}(BF_4)_4$ recorded over 13 h. The first heating process results in a weight loss greater than the subsequent 9 cycles. This can be associated with loss of co-crystallized solvent. The formulation of one sample fits best to $\mathbf{2a}(BF_4)_4 \cdot 5H_2O \cdot MeOH$ according to elemental analysis, so this is reasonable. Over the next 9 cycles we see only a marginal decrease in reversibility in O_2 uptake for each cycle. The weight loss and gain on the final cycle amounts to a 92.9% yield if assuming that the sample is fully desolvated and deoxygenated, *i.e.*, near stoichiometric. Re-sorption of O_2 is significantly slower for the triflate and nitrate salts for which colour change from pink back to dark brown occurs over hours to days. The enthalpy of O_2 binding to the structurally equivalent $Co(II)_2$ sites should be almost identical for each complex, so the difference relates to inaccessibility of O_2 binding sites, as reflected by slow kinetics.

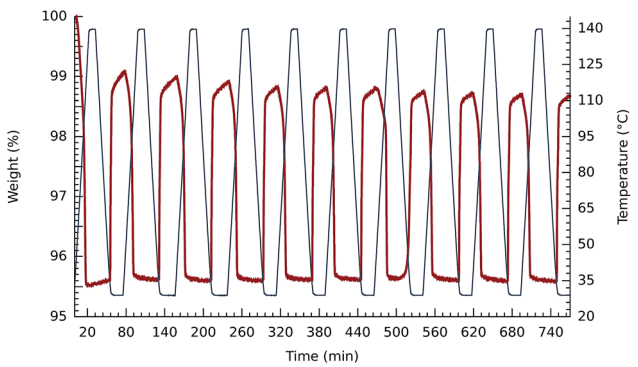

Fig. 2 Temperature dependent cycling of reversible O_2 binding by $\mathbf{2a}(BF_4)_4$ measured using TGA.

Clearly the counteranions influence the O_2 sorption/desorption properties. Thus in our next experiments we kept the counteranion constant, choosing nitrate for which the slowest re-sorption of O_2 was observed. We then chemically tweaked the supporting ligand system by varying substituents on the bridging di-carboxylato linkers, **2a–d**. Our prediction, based on the solution chemistry of **1a–e** was that by introducing electron withdrawing groups onto the supporting scaffold, we would lower the O_2 affinity, further than that already achieved by using nitrate as a counteranion, potentially by orders of magnitude. We therefore expected that the nitrate salt of tetrafluoride substituted bdc^{2-}-bridged complex, **2d**, would show the lowest O_2 affinity of the series. For reference, the isolation of **1e** required −20 °C and an O_2 atmosphere.[11] The intention was to increase the chances for structural characterization of a deoxy form of these materials. Fig. 3 shows that the difference in O_2 release temperatures of the series of nitrate salts of **2a–d** is, however, marginal. So this attempt at the rational design of the active molecular component of a functional solid state material did not meet our expectations and confirmed that aspects of

crystal phase play a major role. The weight losses correspond to a minimum of stoichiometric loss of two O_2 molecules per tetracobalt unit, however, the concurrent release of unknown amounts of solvent makes direct analysis difficult. Inflexion points in the weight loss curves for the materials containing **2a**, **2b** and **2c** would suggest the loss of two chemically different species consistent with water and O_2. These losses occur just under 100 °C and distinguishing the order of loss has not been possible.

Crystal structure of a deoxy complex

The affinity of the PF_6^- salt of the complex $\mathbf{2a_{deoxy}}$ towards O_2 is approximately 10 times greater in the solid state compared to its O_2 affinity in solution. In the absence of a crystal structure of the deoxy form of any member of this series, we attributed this effect to the formation of more reactive coordinatively unsaturated five-coordinated Co(II) sites on deoxygenation. Accordingly we assumed that the relative stabilization of the deoxy form in solution is due to solvent (acetonitrile, acetone or methanol) coordination to the Co(II) sites, which would then remain six coordinated. The solvent ligands would inhibit O_2 binding in both dissociative and associative mechanisms. DFT calculations supported this hypothesis.[10]

Although we have precipitated solid compounds for several members of series **1** and **2** and related hexacobalt systems under dioxygen-free atmospheres,[14] none of these air-sensitive materials have formed single crystals suitable for X-ray diffraction analysis. The increased stability of the nitrate and triflate salts of these deoxy complexes prompted further effort in this direction. We were, however, unable to grow single crystals of the compounds under anaerobic conditions using either *ab initio* preparations, or crystallizations from deoxygenated solutions. Fortunately, upon careful heating to approximately 100 °C, single crystals of $[\{(bpbp)Co_2(O_2)\}_2(NH_2bdc)](NO_3)_4\cdot xH_2O$ ($\mathbf{2b}(NO_3)_4\cdot xH_2O$) change colour from near black to reddish pink, with many of them remaining intact (Fig. 4). Cracking was observed in some crystals, especially larger specimens. This must be due to large strain caused by thermal stress and the molecular movement requisite for desolvation and deoxygenation. When cooled to room temperature and left exposed to oxygen, the crystals slowly reabsorb O_2 over a period between 24 and 48 h depending on size. Even during the resorption of oxygen many of the single crystals did not lose integrity. Through successive X-ray diffraction data collections on *one single crystal* as its oxy, then deoxy, then oxy form again, we can now not only report the first structure of a deoxy form of this type of complex, $[\{(bpbp)Co_2(NO_3)\}_2(NH_2bdc)](NO_3)_2\cdot 2H_2O$, $\mathbf{2b_{deoxy}}(NO_3)_2\cdot 2H_2O$, but also that this material has formed by a remarkable single-crystal-to-single-crystal (SC-to-SC) transformation. It can then undergo a second equally remarkable SC-to-SC to reform the oxy complex. Crystal structures were recorded in all three steps on one crystal, amounting to 1.5 desorption/sorption cycles and $\mathbf{2b_{deoxy}}(NO_3)_2\cdot 2H_2O$ is the middle phase of a SC-to-SC-to-SC transformation (Table 1). Diffraction quality decreased over successive cycles, although visual inspection with a light microscope suggests that good crystals can repeat this process consecutively through at least 5 cycles. They will typically lose integrity, but not crystallinity, after a few cycles, making X-ray diffraction analysis using our machine impossible. Functionality is not lost since the resultant crystalline powders can still reversibly bind O_2.

Fig. 4 Light microscope image of SC-to-SC deoxygenation of $[\{(bpbp)Co_2(O_2)\}_2(NH_2bdc)](NO_3)_4\cdot 7H_2O$, ($\mathbf{2b}(NO_3)_4\cdot 7H_2O$) (left) to give $[\{(bpbp)Co_2(NO_3)\}_2(NH_2bdc)](NO_3)_2\cdot 2H_2O$, $\mathbf{2b_{deoxy}}(NO_3)_2\cdot 2H_2O$ (right). Transformation performed by heating for approximately 5 minutes on a regular hot-plate set to a temperature of 80 °C.

Crystals of $\mathbf{2b}(NO_3)_4\cdot xH_2O$ are weakly diffracting, leading to low quality intensity data, and considerable disorder in both co-crystallized solvent molecules and nitrate counteranions is observed. After heating and the structure of the resultant pink deoxy form had been determined, this same crystal was carefully placed in a drop of Fomblin® Y oil on a microscope slide and left for 48 h whereupon it converted back to the dark colour. Another data set was collected and the re-formation of the $\mathbf{2b}(NO_3)_4\cdot 7H_2O$ verified. The structures of the cations in $\mathbf{2b}(NO_3)_4\cdot 7H_2O$ and $\mathbf{2b_{deoxy}}(NO_3)_2\cdot 2H_2O$ are shown in Fig. 5a and b respectively. Important distances and angles are given in Table 2.

The peroxide ligand is, as expected, absent in the deoxy form. The surprise to us was that the Co(II) ions are still six coordinated. Two of the formally counter anionic nitrate ions are now coordinated in a bridging mode. The coordinated nitrates and peroxo ligands of the deoxy and oxy forms respectively are located on opposite sides of the plane formed by the $Co_4(NH_2bdc)$ unit. Although impossible to decipher which two of the four nitrate anions move and become coordinated in the deoxy form, it is reasonable to assume that it is those in closest proximity to the binding sites at each end of the molecule. A comparison of the oxy and deoxy structures suggest that the translational movement needed for the pertinent O atoms of the closest nitrate ions to each end of the molecule are between 4–6 Å. These closest nitrate oxygen atoms (those associated with N14 and N15) to each dinuclear site are located on the opposite side of the molecule from each other (as defined by the plane of the linking aminobenzene ring). The $O_{NO_3}\cdots Co$ distances are O14···Co1, 5.597 Å O16···Co2, 4.648 Å, O11···Co4, 5.56 Å and O12···Co3, 4.201 Å, ESI Fig. S1.† Thus a scenario for the deoxygenation reaction mechanism of a SN_2 type reaction at each Co ion where the nitrates push the O_2 release can be envisaged. This scenario involves some donor atom slipping and movement of the supporting ligands. An impression of the movement of the atoms of the dinucleating ligand can be seen in the overlay of **2b** and $\mathbf{2b_{deoxy}}$ in ESI Fig. S2.† Relative to the

Table 1 Selected crystallographic data collected on a single crystal after the second and third phase transition

	$[\{(bpbp)Co_2(O_2)\}_2(NH_2bdc)](NO_3)_4\cdot 7H_2O$	$[\{(bpbp)Co_2(NO_3)\}_2(NH_2bdc)](NO_3)_2\cdot 2H_2O$
Empirical formula	$C_{80}H_{97}Co_4N_{17}O_{29}$	$C_{80}H_{87}Co_4N_{17}O_{20}$
Formula weight (g mol^{-1})	1996.48	1842.41
Temperature (K)	150.0(2)	150.0(2)
Crystal system	Triclinic	Triclinic
Space group	$P\bar{1}$	$P\bar{1}$
a (Å)	10.1905(13)	10.8710(9)
b (Å)	21.156(3)	20.7504(19)
c (Å)	22.015(3)	21.3627(15)
α (°)	115.123(4)	64.984(2)
β (°)	92.484(5)	86.763(4)
γ (°)	99.306(5)	79.326(3)
Volume (Å^3)	4207.3(10)	4290.0(6)
Z	2	2
ρ_{calc} (mg mm^{-3})	1.562	1.421
Abs. coefficient	0.869	0.839
$F(000)$	2038.0	1894.0
Crystal size (mm^3)	0.37 × 0.14 × 0.05	0.37 × 0.14 × 0.05
2Θ range for data collection	4.12 to 49.426°	7.03 to 50.054°
Index ranges	$-11 \le h \le 11$, $-24 \le k \le 20$, $-25 \le l \le 25$	$-12 \le h \le 11$, $-22 \le k \le 24$, $-25 \le l \le 25$
Reflections collected	40 936	50 854
Independent reflections	14 235 ($R_{int} = 0.0498$)	15 069 ($R_{int} = 0.0483$)
Data/restraints/parameters	14 235/37/1168	15 069/0/1115
GooF on F^2	1.075	1.062
Final $R_1(F)^a(I > 2\sigma(I))$/w$R_2(F^2)^b$	0.1007/0.2604	0.1024/0.2499
$R_1{}^a$/w$R_2(F^2)^b$ (all data)	0.1525/0.2960	0.1547/0.2820
Largest diff. peak/hole/e Å^{-3}	1.80/−1.33	2.43/−0.92

^{a} $R_1(F) = \sum(||F_o| - |F_c||)/\sum|F_o|$. ^{b} $wR_2(F^2) = \{\sum[w(F_o^2 - F_c^2)^2]/\sum[w(F_o^2)^2]\}^{1/2}$.

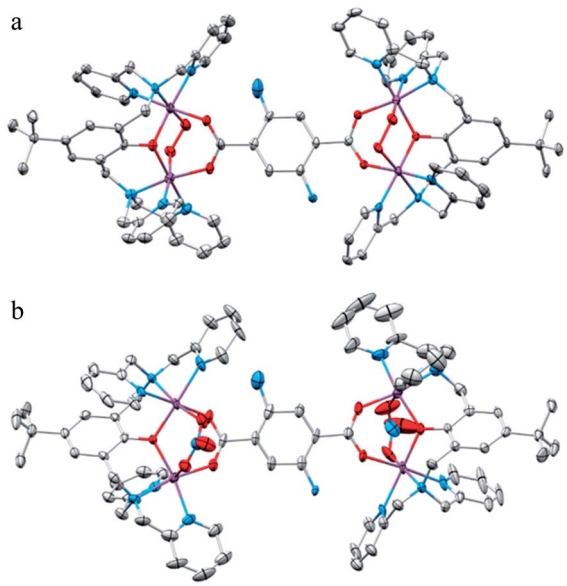

Fig. 5 Molecular structure of the cations in (a) $[\{(bpbp)Co_2(O_2)\}_2(NH_2bdc)](NO_3)_4\cdot 7H_2O$, **2b**$(NO_3)_4\cdot 7H_2O$, (b) $[\{(bpbp)Co_2(NO_3)\}_2(NH_2bdc)](NO_3)_2\cdot 2H_2O$, **2b**$_{deoxy}(NO_3)_2\cdot 2H_2O$. Two amine nitrogen atoms are shown on the 2-aminoterephtalato linker due a 50% occupancy in both positions. Hydrogen atoms omitted for clarity. Anisotropic displacement parameters drawn at the 30% probability level.

Table 2 Selected bond distances (Å) within one of the two dimetallic centers

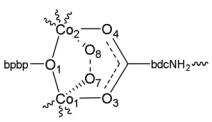

	2b$(NO_3)_4\cdot 7H_2O$	**2b**$_{deoxy}(NO_3)_2\cdot 2H_2O$
Co1–O1	1.895(6)	1.996(5)
Co2–O1	1.894(7)	2.011(5)
Co1–O7 (O_2^{2-}/NO_3^-)^a	2.011(5)	2.271(6)
Co2–O8 (O_2^{2-}/NO_3^-)^a	1.879(7)	2.100(6)
Co1–O3	1.934(6)	1.990(5)
Co2–O4	1.904(6)	2.106(5)
O7–O8 (O_2^{2-}/NO_3^-)^a	1.416(9)	2.212(9)
Co1–Co2	3.164(2)	3.424(1)

^{a} O7 and O8 belong to O_2^{2-} or bridging NO_3^-. For a full list of bond distances and angles see ESI Table S1.

movement of O_2, nitrate and water, this must be a minor rattling for the crystals. It does not, however, lessen the impressiveness of the SC-to-SC transformations observed. The distance between the nitrate coordinated oxygen atoms are on average 2.185(7) Å, whereas the O–O bond distance is av. 1.423(9) Å. The Co(II)–Co(II) distance in **2b**$_{deoxy}$ averages 3.448(2) Å, and this is shortened to a Co(III)–Co(III) distance of av. 3.171(2) Å in the oxygenated form, **2b**. This difference is due to

the bite of the *syn*-μ_2-nitrate^{2-} *vs.* that of *syn*-μ_2-O_2^{2-}, the respective metal ion radii, and the more powerful geometric preference for the Co(III) system to show a regular octahedral geometry. Chemically, each end of **2b** and $\mathbf{2b_{deoxy}}$ is different due to the single amine group *ortho* to one of the carboxylato groups in the linker 2-aminoterephthalato ligand. In both of the structures this amine group is disordered approximately equally over the two positions *para* to each other (both positions depicted in Fig. 5). There is H-bonding between the NH_2bdc^{2-} amine group and the adjacent coordinated carboxylato oxygen atom (O···N = 2717 Å, 2.808 Å in $\mathbf{2a_{deoxy}}$ 2.697 Å, 2.723 Å in **2a**).

Inspection of unit cell sizes reveals that the crystal lattice expands by around 2% when it expels O_2. This is surprising given that the material is being converted from a tetracation to a dianion with correspondingly four and two counter nitrates respectively, and a lower water content in the deoxy from. The calculated void space in fully desolvated models of $\mathbf{2b}(NO_3)_4\cdot 7H_2O$ and $\mathbf{2b_{deoxy}}(NO_3)_2\cdot 2H_2O$ using a probe radius of 1.2 Å are 4.8% and 7.0% respectively. Another possible contributing factor for the relatively slow uptake of O_2 by the nitrate salt is that the voids do not form channels in $\mathbf{2b_{deoxy}}$-$(NO_3)_2\cdot 2H_2O$. By contrast they do in $\mathbf{2b}(NO_3)_4\cdot 7H_2O$. This might facilitate the desorption process. If the probe radius is expanded to 1.6 Å for $\mathbf{2b}(NO_3)_4\cdot 7H_2O$ and 1.9 Å for $\mathbf{2b_{deoxy}}$-$(NO_3)_2\cdot 2H_2O$ the void space effectively becomes 0% in both structures (calculated within the Mercury CSD 3.1.1 suite from CCDC[15,16]). The kinetic diameter of O_2 is 3.46 Å.[17] See ESI Fig. S6–S9† for impressions of voids/pseudo voids. These facts suggest an active transport mechanism for the O_2 where conduit voids are not actually essential for sorption/desorption. We have shown that significant atomic movement is possible in the crystals and we conclude that the O_2 hops between the chemisorptive binding sites. The pronounced structural flexibility observed here upon guest desorption is reminiscent of that seen in a range of other discrete supramolecular host materials,[18,19] in which retention of monocrystallinity occurs despite the rather extreme requirements that guest molecule migration and structural transformation place on the host crystal. Host materials have been shown to undergo phase transitions from non-porous to porous on uptake of CO_2.[19] Of particular note here is that the system retains crystallinity with the migration and subsequent binding of nitrate anions on the dinuclear Co(II) sites (see ESI Fig. S2(b)† for molecular overlays showing the resulting distortion of the discrete tetranuclear host).

The hydrogen bonding interaction of the amine group with the coordinated carboxylate at one end of the molecule might be expected to modulate the O_2 binding affinity of this end such that the semioxy intermediate, $[(bpbp)Co_2(NO_3)(NH_2bdc)(bpbp)$-$Co_2(O_2)](NO_3)_3$, is thermally stable at intermediate temperatures. We have, however, not found conditions by which we can detect this putative species during attempts to follow the single crystal structure of a sorbing crystal. We note that the temperature dependent cycling of reversible O_2 binding by $\mathbf{2b}(BF_4)_4$ (Fig. S10†) shows yields decrease marginally more on each successive cycle compared to $\mathbf{2a}(NO_3)_4$ (Fig. 2). It seems obvious to speculate that the BF_4^- ions do not interact with the Co(II)$_2$ sites as intimately as NO_3^-. Thus on O_2 desorption lattice water coordinates to the resultant Co(II) ions. If the aquo ligands of these putative $\{Co(II)(OH_2)\}_2$ motifs cannot be substituted by O_2 during its oxidative sorption, "met" Co_2^{III} sites containing aquo and hydoxo ligands will result through an outersphere oxidation process. We have observed previously that reduction of complexes with this H-bonded $Co^{III}(HOHOH)Co^{III}$ motif is not favorable,[13] thus the active sites will be poisoned.

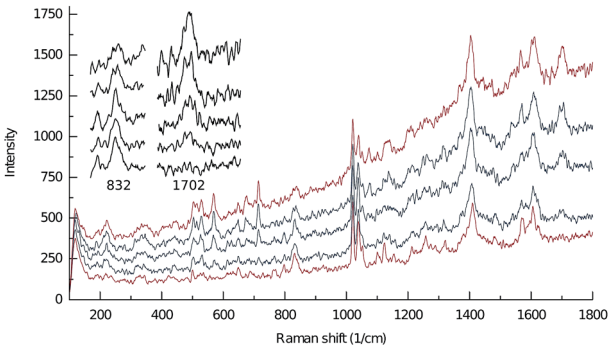

Fig. 6 Raman spectra from 100 to 1800 cm^{-1} following thermal deoxygenation of $[\{(bpbp)Co_2(O_2)_2\}(NH_2bdc)](NO_3)_4\cdot 7H_2O$, $\mathbf{2b}(NO_3)_4\cdot 7H_2O$ at 20 °C, 70 °C, 90 °C, 100 °C and 120 °C (from bottom to top).

Vibrational spectroscopy

The solid state transformations between $\mathbf{2b}(NO_3)_4\cdot 7H_2O$ and $\mathbf{2b_{deoxy}}(NO_3)_2\cdot 2H_2O$ can be observed using resonance Raman and IR spectroscopies (Fig. 6 and 7, respectively). Specifically, the band at 840 cm^{-1}, assigned to the O–O stretch, is much reduced in the resonance Raman spectra when $\mathbf{2b}(NO_3)_4\cdot 7H_2O$ is heated. During this process new bands associated with the coordinated bridging nitrate at 570, 710 and 1700 cm^{-1} grow in.

IR spectra show that water is lost in the first heating of $\mathbf{2b}(NO_3)_4\cdot 7H_2O$ as the broad band between 3000 and 3500 cm^{-1} reduces significantly, see SI Fig. S3.† Otherwise the most significant changes occur between 800 and 1000 cm^{-1} and these can predominantly be associated with changes in the N–O bond strength within the nitrate ions, especially those moving from coordinated to non-coordinated positions. The two coordinated

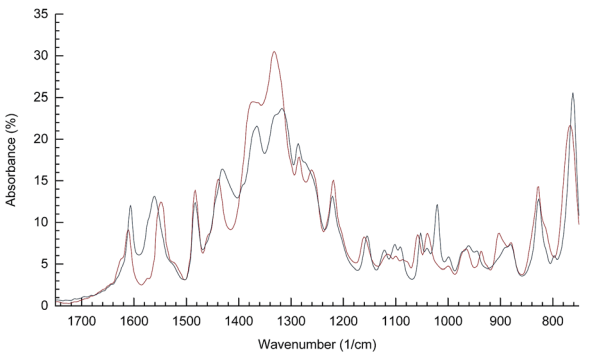

Fig. 7 FT-IR spectra from 1650 cm^{-1} to 850 cm^{-1} of $\mathbf{2b_{deoxy}}(NO_3)_2\cdot 2H_2O$, $T = 120$ °C (red) and $\mathbf{2b}(NO_3)_4\cdot 7H_2O$, $T = -20$ °C (black).

nitrates can be expected to be chemically different due to the presence of the amine adjacent to one of these and this will smear the spectra further. A small difference in the ν_{as} (*ca.* 1570 cm^{-1}) and ν_s (*ca.* 1440 cm^{-1}) due to the bridging carboxylato bands of the NH_2bdc^{2-} unit can be seen in the IR spectra of the oxy and deoxy forms. This is rationalized mainly by the observed changes in the C–O bond distances in the Co(II) and Co(III) complexes.

Conclusions

With the *cleavage of four bonds, and the creation of four bonds in one molecule/cation*, the complete evacuation and *selective* uptake of a diatomic gas, atom *movements by up to* 7 Å of anions, hydration changes and donor atom sliding, the *successive* SC-to-SC-to-SC transformations we have followed by single crystal X-ray diffraction are remarkable. Although several impressive examples of SC-to-SC transformations are known,[18–20] to our knowledge none undergo such extensive atom movements, bond cleavage and formation and reversibility with gas sorption and desorption.

Previously we had speculated that the active site of $\mathbf{2a_{deoxy}}(PF_6)_4$ in the *solid state* was coordinatively unsaturated and that this accounted for a higher affinity, by an order of magnitude, for O_2 compared to when $\mathbf{2a_{deoxy}}$ is dissolved and hence having solvent molecules occupying the sixth position.[8] The present work shows this assumption may not be entirely correct: The respective degrees of association of the counter-anions of the series with the Co(II) atoms of the deoxy forms play a major role in determining reaction rates of sorption and desorption processes. Nitrate is the strongest donor of the counteranions selected in this study, thus it will form the strongest interaction (formally coordination) with the metal ions. The fluorinated anions, typically regarded as non-coordinating or very weakly coordinating,[21] are presumably more weakly associated with the metal centers in the deoxy forms, if they move at all during the sorption/desorption processes.

In the solid state this series of compounds show O_2 binding affinities and reversibility which rival that of myoglobin. We have found, however, that *crystal structure* plays a far greater role in tuning these properties compared with the electronic tuning possible through the introduction of substituents on the linker dicarboxylate unit. BET measurements of $\mathbf{2a_{deoxy}}(PF_6)_4$ had indicated that this material was non-porous.[8] This result, along with the calculated insufficient void space in $\mathbf{2b_{deoxy}}(NO_3)_2\cdot 2H_2O$ for physisorbing O_2 implies that the O_2 molecules are actively transported through the crystalline phases of these materials: a biomimetic chemisorptive hopping mechanism of the O_2 molecules from Co_2 site to Co_2 site can be imagined. This will require considerable molecular flexibility, molecule and nitrate ion movement, yet crystallinity is retained.

Experimental

ESI-MS spectra were recorded on a Bruker microTOF-QII. Thermogravimetric analysis was performed on a PerkinElmer TGA 4000. Samples were heated from 30 °C to 140 °C at 5 °C min^{-1} under a stream of N_2 (20.0 mL min^{-1}). Cooling was done at same rate under a stream of O_2 (20.0 mL min^{-1}). VT-IR measurements were collected from 25 °C up to 240 °C (ramping and then holding at each temperature) and then back down again to RT using a Bruker FT-IR spectrometer with ATR attachment. VT-Raman was performed between −20 °C and 120 °C using a Renishaw Raman in Via Reflex spectrometer (514 nm laser). Elemental microanalyses were performed at the Department of Chemistry, University of Copenhagen, Denmark. Single crystal data were collected with a Bruker-Nonius X8 Kappa Apex II at 150 K using Mo Kα radiation ($\lambda = 0.71073$ Å). Semi-empirical absorption corrections were applied using SADABS.[22] Initial models were obtained with SHELXS-2013 using Direct Methods and further refined with SHELXL-2013.[23] Hydrogen atoms on C atoms were placed at calculated positions and allowed to ride during refinement with $U_{iso}(H) = 1.5U_{eq}$ when connected to methyl groups and $U_{iso}(H) = 1.2U_{eq}$ for others. Hydrogen atoms connected to heteroatoms were not located in different Fourier maps and were excluded in the refinement. $[\{Co_2(bpbp)(O_2)\}_2(bdc)](PF_6)_4\cdot 3H_2O$ ($\mathbf{2a}(PF_6)_4\cdot 3H_2O$) and bpbpH were prepared as previously reported.[8,24]

Synthesis

$[\{Co_2(bpbp)(O_2)\}_2(bdc)](BF_4)_4\cdot 5H_2O\cdot MeOH$ ($\mathbf{2a}(BF_4)_4\cdot 5H_2O\cdot MeOH$). A solution of sodium 1,4-benzenedicarboxylate (Na_2bdc; 55.0 mg, 0.26 mmol) was dissolved in H_2O (10 mL) and added dropwise to a solution of $Co(BF_4)_2\cdot 6H_2O$ (356.7 mg, 1.05 mmol) and bpbpH (299.8 mg, 0.52 mmol) in acetone–MeOH (1 : 1, 50 mL). Slow evaporation of the resulting dark brown solution yielded black needle-like crystals which were collected by filtration, washed with ice cold H_2O (3 × 5 mL) and air-dried (289.7 mg, 0.15 mmol, 57.0%). Anal. calcd (found) for $C_{81}H_{96}B_4Co_4F_{16}N_{12}O_{16}$ (2076.65 g mol^{-1}): C, 46.85 (46.19); H, 4.66 (4.20); N, 8.09 (7.98)%. ESI-MS (MeCN, pos. mode) calcd (found) m/z = 427.10 (427.10, $[Co_2(bpbp)(bdc)]^{2+}$, $C_{44}H_{44}Co_2N_6O_5$, 100%). IR (FT-ATR diamond anvil) ν/cm^{-1} = 1611 (m), 1554 (m), 1482 (m), 1439 (m), 1385 (s), 1313 (w), 1285 (m), 1265 (w), 1222 (m), 1161 (w), 1041 (s), 935 (m), 874 (m), 824 (m), 770 (s), 736 (m), 714 (m), 696 (w), 519 (m), 458 (s).

$[\{Co_2(bpbp)(O_2)\}_2(bdc)](NO_3)_4\cdot 15H_2O$ ($\mathbf{2a}(NO_3)_4\cdot 15H_2O$). Prepared as above but using $Co(NO_3)_2\cdot 6H_2O$ yielding black needle-like crystals (370.2 mg, 0.20 mmol, 76.7%). Anal. calcd (found) for $C_{80}H_{114}Co_4N_{16}O_{38}$ (2143.60 g mol^{-1}): C, 44.83 (44.63); H, 5.36 (4.22); N, 10.45 (10.26)%. ESI-MS (MeCN, pos. mode) calcd (found) m/z = 427.10 (427.10, $[Co_2(bpbp)(bdc)]^{2+}$, $C_{44}H_{44}Co_2N_6O_5$, 100%). IR (FT-ATR diamond anvil) ν/cm^{-1} = 1611 (m), 1554 (s), 1487 (s), 1430 (m), 1324 (s), 1218 (s), 1157 (m), 1109 (w), 1055 (m), 1039 (m), 969 (w), 937 (w), 903 (w), 876 (m), 827 (s), 763 (s), 741 (s), 720 (m).

$[\{Co_2(bpbp)(O_2)\}_2(bdc)](OTf)_4\cdot 5H_2O$ ($\mathbf{2a}(OTf)_4\cdot 5H_2O$). Prepared as above but from $Co(OTf)_2$ yielding black needle-like crystals (273.1 mg, 0.12 mmol, 47.7%). Anal. calcd (found) for $C_{84}H_0Co_4F_{12}N_{12}O_{27}S_4$ (2293.67 g mol^{-1}): C, 43.99 (43.91); H, 4.04 (3.59); N, 7.33 (7.27)%. ESI-MS (MeCN, pos. mode) calcd (found) m/z = 427.10 (427.10, $[Co_2(bpbp)(bdc)]^{2+}$, $C_{44}H_{44}Co_2N_6O_5$, 65%), IR (FT-ATR diamond anvil) ν/cm^{-1} =

1606 (w), 1543 (m), 1484 (m), 1432 (w), 1383 (m), 1254 (s), 1218 (m), 1139 (m), 1059 (w), 1028 (s), 879 (w), 822 (m), 763 (s), 718 (w), 653 (s), 569 (m), 512 (s).

[{Co_2(bpbp)(O_2)}$_2$(NH_2bdc)](NO_3)$_4$·11H_2O (2b(NO_3)$_4$·11H_2O). 2-Aminoterephthalic acid (102.0 mg, 0.56 mmol) was added to a solution of NaOH (45.0 mg, 1.13 mmol, 2 eq.) in H_2O (25 mL) and the mixture was gently heated until a clear solution formed whereupon it was added dropwise to a mixture of $Co(NO_3)_2\cdot 6H_2O$ (655.5 mg, 2.25 mmol) and bpbpH (645.0 mg, 1.13 mmol) in acetone–MeOH (2 : 1, 75 mL). Slow evaporation of the resulting dark brown solution yielded black needle-like crystals which were collected by filtration, washed with ice cold H_2O (3 × 5 mL) and air-dried (979.3 mg, 0.52 mmol, 93.5%). Anal. calcd (found) for $C_{80}H_{105}Co_4N_{17}O_{33}$ (2068.52 g mol^{-1}): C, 46.45 (46.38); H, 5.12 (4.53); N, 11.51 (11.53)%. ESI-MS (MeCN, pos. mode) calcd (found) m/z = 434.61 (434.61, $[Co_2(bpbp)(NH_2bdc) + H^+]^{2+}$, $C_{44}H_{45}Co_2N_7O_5$, 96%), 868.21 (868.20, $[Co_2(bpbp)(NH_2bdc)]^+$, $C_{44}H_{44}Co_2N_7O_5$, 100%), 931.20 (931.20, $[Co_2(bpbp)(NH_2bdc) + NO_3^-]^+$, $C_{44}H_{45}Co_2N_8O_8$, 29%). IR (FT-ATR diamond anvil) ν/cm^{-1} = 1604 (m), 1545 (m), 1484 (m), 1435 (m), 1331 (s), 1218 (m), 1143 (w), 1041 (w), 967 (w), 883 (w), 829 (m), 766 (s), 720 (w).

[{Co_2(bpbp)(O_2)}$_2$(Cl_2bdc)](NO_3)$_4$·12H_2O (2c(NO_3)$_4$·12H_2O). 2,5-Dichloroterephtalic acid (112.8 mg, 0.48 mmol) was added to a solution of NaOH (38.4 mg, 0.96 mmol, 2 eq.) in H_2O (10 mL) and the mixture was gently heated until a clear solution formed whereupon it was added dropwise to a mixture of $Co(NO_3)_2\cdot 6H_2O$ (558.8 mg, 1.92 mmol) and bpbpH (549.4 mg, 0.96 mmol) in acetone–MeOH (3 : 1, 100 mL). Slow evaporation of the resulting dark brown solution yielded black needle-like crystals which were collected by filtration, washed with ice cold H_2O (3 × 5 mL) and air-dried (575.2 mg, 0.30 mmol, 62.0%). Anal. calcd (found) for $C_{80}H_{104}Cl_2Co_4N_{16}O_{34}$ (2140.41 g mol^{-1}): C, 44.89 (44.89); H, 4.90 (4.36); N, 10.47 (10.43)%. ESI-MS (MeCN, pos. mode) calcd (found) m/z = 461.07 (461.06, $[Co_2(bpbp)(Cl_2bdc) + H^+]^{2+}$, $C_{44}H_{42}Cl_2Co_2N_6O_5$, 50%), 472.05 (472.05, $[Co_2(bpbp)(Cl_2bdc) + Na^+]^{2+}$, $C_{44}H_{41}Cl_2Co_2N_7NaO_5$, 17%), 921.13 (921.11, $[\{Co_2(bpbp)\}_2(Cl_2bdc) + 2Na^+ + 3NO_3^-]^{2+}$, $C_{80}H_{80}Cl_2Co_4Na_2N_{15}O_{15}$, 15%), 922.13 (922.11, $[Co_2(bpbp)(Cl_2bdc) + H^+]^{1+}$, $C_{44}H_{42}Cl_2Co_2N_6O_5$, 30%), 984.11 (984.11, $[Co_2(bpbp)(Cl_2bdc) + H^+ + NO_3^-]^{1+}$, $C_{44}H_{42}Cl_2Co_2N_7O_8$, 11%). IR (FT-ATR diamond anvil) ν/cm^{-1} = 1611 (m), 1566 (m), 1480 (m), 1331 (s), 1215 (m), 1152 (w), 1084 (w), 1044 (w), 912 (w), 831 (m), 770 (s), 720 (m).

[{Co_2(bpbp)(O_2)}$_2$(F_4bdc)](NO_3)$_4$·18H_2O (2d(NO_3)$_4$·18H_2O). Tetrafluoroterephtalic acid (114.3 mg, 0.48 mmol) was added to a solution of NaOH (38.4 mg, 0.96 mmol, 2 eq.) in H_2O (15 mL) and the mixture was gently heated until a clear solution formed whereupon it was added dropwise to a mixture of $Co(NO_3)_2\cdot 6H_2O$ (558.8 mg, 1.92 mmol) and bpbpH (549.8 mg, 0.96 mmol) in acetone–H_2O (1 : 1, 50 mL) whereupon a precipitate formed. Acetone was added until a clear solution formed (approximately 50 mL) and the reaction mixture was stirred at room temperature for approximately 7 days whereupon it had turned into a slightly gelatinous appearance. Filtration through celite yielded a clear dark brown solution which upon slow evaporation gave black needle-like crystals which were collected by filtration, washed with H_2O (3 × 5 mL) and air-dried (622.3 mg, 0.32 mmol, 67.3%). Anal. calcd (found) for $C_{80}H_{114}Co_4F_4N_{16}O_{40}$ (2251.57 g mol^{-1}): C, 42.67 (42.82); H, 5.10 (4.49); N, 9.95 (9.95)%. ESI-MS (MeCN, pos. mode) calcd (found) m/z = 463.09 (463.08, $[Co_2(bpbp)(F_4bdc) + H^+]^{2+}$, $C_{44}H_{40}Co_2F_4N_6O_5$, 80%), 925.16 (925.16, $[Co_2(bpbp)(F_4bdc)]^+$, $C_{44}H_{39}Co_2F_4N_6O_5$, 94%). IR (FT-ATR diamond anvil) ν/cm^{-1} = 1587 (m), 1480 (m), 1437 (m), 1330 (s), 1213 (m), 1160 (m), 1091 (w), 1057 (w), 996 (m), 907 (w), 828 (m), 749 (s).

Acknowledgements

This work was supported by the Danish Council for Independent Research|Natural Sciences. LJC would like to thank Dr Elizabeth Carter for help with VT IR and VT Raman measurements. JS would like to thank Dr Jason Price and Prof. Mikael Håkansson for help with an initial X-ray structural data collections.

Notes and references

1 T. R. Gaffney, *Curr. Opin. Solid State Mater. Sci.*, 1996, **1**, 69–75.

2 (*a*) S. Sircar, M. B. Rao and T. C. Golden, in *Adsorption and Its Applications in Industry and Environmental Protection, Vol I: Applications in Industry*, Elsevier Science Publ B V, Amsterdam, 1999, vol. 120, pp. 395–425; (*b*) M. W. Ackley, S. U. Rege and H. Saxena, *Microporous Mesoporous Mater.*, 2003, **61**, 25; (*c*) M. Moliner, C. Mártinez and A. Corma, *Chem. Mater.*, 2014, **26**, 246–258.

3 (*a*) M. Suzuki, T. Ishiguro, M. Kozuka and K. Nakamoto, *Inorg. Chem.*, 1981, **20**, 1993–1996; (*b*) G. Q. Li and R. Govind, *Ind. Eng. Chem. Res.*, 1994, **33**, 755–783.

4 (*a*) L. Vaska, *Science*, 1963, **140**, 809–810; (*b*) H. Lebel, C. Ladjel, F. Bélanger-Gariépy and F. Schaper, *J. Organomet. Chem.*, 2008, **693**, 2645–2648.

5 (*a*) L. Vaska, *Acc. Chem. Res.*, 1976, **9**, 175–183; (*b*) E. C. Niederhoffer, J. H. Timmons and A. E. Martell, *Chem. Rev.*, 1984, **84**, 137–203.

6 (*a*) H. Nishide, T. Suzuki, R. Nakagawa and E. Tsuchida, *J. Am. Chem. Soc.*, 1994, **116**, 4503–4504; (*b*) N. Preethi, H. Shinohara and H. Nishide, *React. Funct. Polym.*, 2006, **66**, 851–855; (*c*) M. Shoji, K. Oyaizu and H. Nishide, *Polymer*, 2008, **49**, 5659–5664.

7 (*a*) A. C. Sharma and A. S. Borovik, *J. Am. Chem. Soc.*, 2000, **12**, 8946–8955; (*b*) L. L. Welbes and A. S. Borovik, *Acc. Chem. Res.*, 2005, **38**, 765–774; (*c*) R. J. P. Corriu, E. Lancelle-Beltran, A. Mehdi, C. Reyé, S. Brandés and R. Guilard, *J. Mater. Chem.*, 2002, **12**, 1355–1362.

8 P. D. Southon, D. J. Price, P. K. Nielsen, C. J. McKenzie and C. J. Kepert, *J. Am. Chem. Soc.*, 2011, **133**, 10885–10891.

9 L. J. Murray, M. Dinca, J. Yano, S. Chavan, S. Bordiga, C. M. Brown and J. R. Long, *J. Am. Chem. Soc.*, 2010, **132**, 7856–7857.

10 E. D. Bloch, L. J. Murray, W. L. Queen, S. Chavan, S. N. Maximoff, J. P. Bigi, R. Krishna, V. K. Peterson, F. Grandjean, G. J. Long, B. Smit, S. Bordiga, C. M. Brown and J. R. Long, *J. Am. Chem. Soc.*, 2011, **133**, 14814–14822.

11 M. S. Vad, F. B. Johansson, R. Kirk Seidler-Egdal, J. E. McGrady, S. M. Novikov, S. I. Bozhevolnyi, A. D. Bond and C. J. McKenzie, *Dalton Trans.*, 2013, **42**, 9921–9929.
12 H. Wackerbarth, F. B. Larsen, A. Glaargaard Hansen, C. J. McKenzie and J. Ulstrup, *Dalton Trans.*, 2006, 3438–3444.
13 M. Ghiladi, J. T. Gomez, A. Hazell, P. Kofod, J. Lumtscher and C. J. McKenzie, *J. Chem. Soc., Dalton Trans.*, 2003, 1320–1325.
14 F. B. Johansson, A. D. Bond and C. J. McKenzie, *Inorg. Chem.*, 2007, **46**, 2224–2236.
15 (*a*) C. F. Macrae, P. R. Edgington, P. McCabe, E. Pidcock, G. P. Shields, R. Taylor, M. Towler and J. van de Streek, *J. Appl. Crystallogr.*, 2006, **39**, 453–457; (*b*) C. F. Macrae, I. J. Bruno, J. A. Chisholm, P. R. Edgington, P. McCabe, E. Pidcock, L. Rodriguez-Monge, R. Taylor, J. van de Streek and P. A. Wood, *J. Appl. Crystallogr.*, 2008, **41**, 466–470.
16 F. H. Allen, *Acta Crystallogr., Sect. B: Struct. Sci.*, 2002, **58**, 380–388.
17 D. W. Breck, in *Zeolite Molecular Sieves: Structure, Chemistry and Use*, John Wiley & Sons, Inc., New York, NY, USA, 1974, pp. 593–724.
18 (*a*) J. Tian, P. Thallapally, J. Liu, G. J. Exarhos and J. L. Atwood, *Chem. Commun.*, 2010, **47**, 701–703; (*b*) W. Yang, A. J. Davies, X. Lin, M. Suyetin, R. Matsuda, A. J. Blake, C. Wilson, W. Lewis, J. E. Parker, C. C. Tang, M. W. George, P. Hubberstey, S. Kitagawa, H. Sakamoto, E. Bichoutskaia, N. R. Champness, S. Yang and M. Schröder, *Chem. Sci.*, 2012, **3**, 2933–2999.
19 (*a*) T. Jacobs, G. O. Lloyd, J.-A. Gertenbach, K. K. Müller-Nedebock, C. Esterhuysen and L. J. Barbour, *Angew. Chem.*, 2012, **124**, 4997–5000; (*b*) T. Jacobs and L. J. Barbour, *CrystEngComm*, 2012, **15**, 1512–1514; (*c*) L. Dobrzańska, G. O. Lloyd, C. Esterhuysen and L. J. Barbour, *Angew. Chem., Int. Ed.*, 2006, **45**, 5856–5859.
20 (*a*) O. V. Zenkina, E. C. Keska, R. Wang and C. M. Crudden, *Angew. Chem., Int. Ed.*, 2011, **50**, 8100–8104; (*b*) C. G. Bezzu1, M. Helliwell, J. E. Warren, D. R. Allan and N. B. McKeown1, *Science*, 2010, **327**, 1627–1630; (*c*) M. Albrecht, M. Lutz, A. L. Spek and G. van Koten, *Nature*, 2000, **406**, 970–974; (*d*) Z. Huang, P. S. White and M. Brookhart, *Nature*, 2010, **465**, 598–601; (*e*) M. A. Garcia-Garibay, *Angew. Chem., Int. Ed.*, 2007, **46**, 8945–8947.
21 M. R. Rosenthal, *J. Chem. Educ.*, 1973, **50**, 331.
22 *SADABS*, Bruker AXS Inc., Madison, Wisconsin, USA, 2001.
23 G. M. Sheldrick, *Acta Crystallogr., Sect. A: Cryst. Phys., Diffr., Theor. Gen. Crystallogr.*, 2008, **64**, 112–122.
24 M. Ghiladi, C. J. McKenzie, A. Meier, A. K. Powell, J. Ulstrup and S. Wocadlo, *J. Chem. Soc., Dalton Trans.*, 1997, **21**, 4011–4018.